A well-structured metastable ceria surface

R. Olbrich,[1] H. H. Pieper,[1] R. Oelke,[1] H. Wilkens,[1] J. Wollschläger,[1] M. H. Zoellner,[2] T. Schroeder,[2] and M. Reichling[1,a)]
[1]*Fachbereich Physik, Universität Osnabrück, Barbarastr. 7, 49076 Osnabrück, Germany*
[2]*IHP, Im Technologiepark 25, 15236 Frankfurt (Oder), Germany*

(Received 10 January 2014; accepted 11 February 2014; published online 25 February 2014)

By the growth of a 180 nm thick film on Si(111), we produce a metastable ceria surface with a morphology dominated by terraced pyramids with an oriented triangular base. Changes in the nanoscale surface morphology and local surface potential due to annealing at temperatures ranging from 300 K to 1150 K in the ultra-high vacuum are studied with non-contact atomic force microscopy and Kelvin probe force microscopy. As the surface is stable in the temperature range of 300 K to 850 K, it is most interesting for applications requiring regular steps with a height of one O-Ce-O triple layer. © *2014 AIP Publishing LLC*. [http://dx.doi.org/10.1063/1.4866667]

Cerium oxide (ceria) is a most important material in heterogeneous catalysis due to several of its properties like superb temperature stability and the ability of the cerium ions to easily be transformed from oxidation state III to IV under oxidation conditions and vice-versa under reducing conditions. Prominent examples for ceria-based catalysis are the water-gas shift reaction and hydrocarbon oxidation,[1] while the most widespread application is the three-way-catalyst developed for the automotive industry.[2] The formation and extinction of oxygen vacancies on the ceria surface is crucial for its high oxygen storage and delivery capacity. Therefore, the details of ceria surface reduction and related electron localisation have recently been topic of numerous experimental and theoretical studies.[3–11] Furthermore, the geometric and electronic structure of step edges on ceria and other fluorite type crystals has recently been studied extensively[12–15] as low-coordinated atoms at step edge and kink sites often enhance the reactivity of catalytic surfaces and provide nucleation sites for deposited metal.[16–18] Here, we introduce a ceria surface prepared by film growth that exhibits an exceptionally rich structure of step edges regularly arranged in terraced pyramids. The film with a thickness of typically 150 nm to 250 nm is grown with a hex Pr_2O_3(0001) buffer layer on Si(111) by molecular beam epitaxy.[19] We reveal the kinetically determined surface morphology of the as-grown film and demonstrate its transformation into the thermodynamic equilibrium morphology known from the surface of the well-prepared (111) bulk ceria surfaces.[20] The as-grown film reveals metastable terraced pyramidal nanostructures on the surface that have much more kink sites and step edges than a well-prepared bulk surface.[20]

The characterization of the film surface is performed with atomic force microscopy operated in the non-contact mode (NC-AFM), a technique that is well suited for high resolution imaging of an insulating oxide surface.[21] NC-AFM studies are performed in an ultra-high vacuum (UHV) system at a base pressure in the low 10^{-10} millibars range. The force microscope is a modified commercial ultrahigh vacuum AFM/STM (Omicron NanoTechnology, Taunusstein, Germany), described in detail earlier[22] that is operated in the constant frequency shift mode where the image contrast represents the topography of the surface.[23] The action of electrostatic forces is minimised during imaging by dynamically adjusting the bias between the tip and conducting sample support to an appropriate value.[24] This allows the detection of variations in the local potential of the ceria surface.[20] Ceria films are grown by molecular beam epitaxy on oriented 4 in. boron-doped Si(111) wafers where the details of the film growth and basic structural properties have been described elsewhere.[19] The wafer is cut in pieces of 2×8 mm^2 that are heated to well defined temperatures prior to NC-AFM measurements. The sample holder, heater and temperature measurement system used for the preparation is outlined in Ref. 25. The surface is prepared in annealing cycles rising the temperature from room temperature to the set-point temperature with procedures and precision in temperature measurement similar to those outlined in Ref. 20. To keep thermal stress low, heating and cooling rates are limited to about 20 K/min. The set-point temperature is kept for 30 min, and afterwards the temperature is ramped down, so that all measurements are performed at room temperature. For one preparation, we additionally apply Ar^+ ion sputtering cycles (1.5 keV ion energy) for 5 min. Most samples are treated with several annealing cycles with increasing set-point temperature, however, some samples are heated directly to only one set-point temperature. We do not find a significant difference in the resulting surface morphology for samples being heated to a certain set-point temperature in one cycle or with several cycles of increasing temperature.

Our study aims at elucidating the surface morphology of the film and its transformations as a function of the heat treatment. NC-AFM measurements reveal two basic types of surface morphology, one found in the temperature range of 300 K to 850 K that is further on referred to as *low temperature morphology* and another one found in the temperature range of 930 K to 1100 K further on referred to as *high temperature morphology*.

Figure 1 is an overview of typical results for the low temperature morphology as obtained by NC-AFM imaging. Images of Figure 1(a) are representative for the as-prepared sample that prevails in its basic structure up to annealing temperatures of 850 K as seen in Figures 1(b)–1(f). The main structural elements are regular, 4 to 6 nm high pyramids with

a)reichling@uos.de

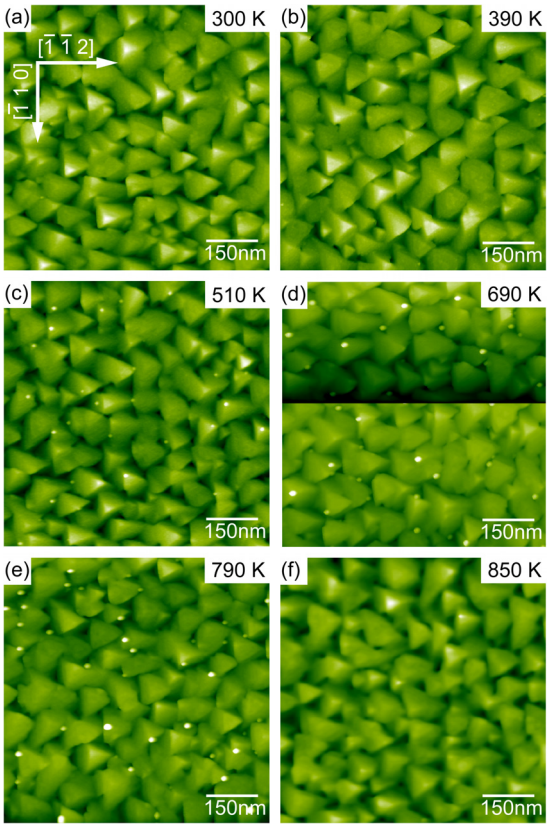

FIG. 1. Selected NC-AFM topography images taken after different post deposition annealing treatments representing the low temperature morphology. (a) Unprepared cerium oxide film; (b)–(f) annealing at 390 K, 510 K, 690 K, 790 K, and 850 K. The in-plane crystallographic directions indicated in (a) are the same for all images of this and the following figures.

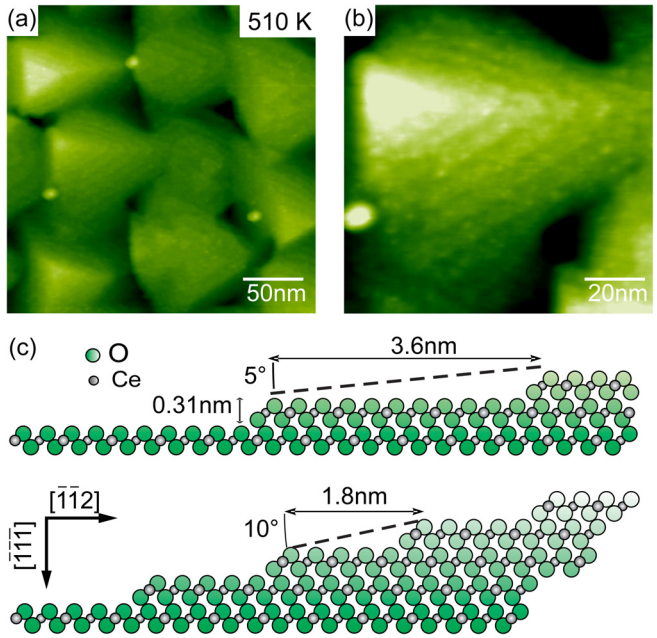

FIG. 2. Detailed NC-AFM study and model structure for pyramids observed in images from Fig. 1. (a) After annealing at 510 K, the terraced formation of the pyramidal faces appears as the layer of volatile contaminants on the film surface is removed. (b) The high magnification image of a pyramidal structure shows the composition of facets of a regular arrangement of terraces separated by steps of one triple-layer (0.31 nm) height. (c) Model for the terraced structure of the top and bottom parts of the pyramidal structures based on a measurement of the height and lateral extension of the pyramids.

a triangular base. The edges of the pyramids have a length of typically 100 nm. As the samples are exposed to air after film growth and, at this stage, they are not further prepared, it is obvious that the pyramidal structures are covered by a contamination layer. By annealing the film to 510 K, some of the contamination can be removed, and the NC-AFM images reveal that the pyramidal faces are built from (111) terraces with details illustrated in Figure 2. For a quantitative analysis of the images, we measure the slope of pyramidal faces and perform a statistical analysis. Within the experimental error, we can identify two different slopes, one for the bottom layers and another one for the top layers of the pyramids. Pyramids grow with a slope of about 10° to the (111) surface plane in the bottom layers and run out with a slope of about 5° in the top layers. Note, however, that most pyramidal structures overlap each other limiting the accuracy of the slope analysis. The layers with a 10° slope can well be associated with a {332} facet while the closest matching facet for the top layers is a {665} facet corresponding to a 4.8° slope and a terrace width of 3.74 nm. In the region with 5° slope, the measured width of the terraces is 3 to 5 nm with a step height of about 0.31 nm corresponding to the height of a O-Ce-O triple layer. Figure 2(c) shows a side view model for the described top and bottom layers of the pyramidal faces along the $[\bar{1}\,\bar{1}\,2]$ direction taking the step edge height of O-Ce-O triple layers into account.

A careful inspection of Figures 1(c)–1(e) reveals the formation of spikes appearing on the surface in the annealing temperature range of about 500 K to about 800 K. These spikes have a width of less than 3 nm but rise above the highest pyramids. To determine the average height and width of the spikes, we analyse cross-sections taken over selected spikes. The density of the spikes and their height increases with annealing temperature where the height reaches a maximum of 9 to 11 nm at 800 K. The origin of the spikes is yet unclear, however, we speculate that they result from contaminants in the film segregated during annealing or material diffusing from the praseodymium oxide buffer layer or silicon substrate to the film surface. This notion is reinforced by the fact that almost all spikes are placed in between pyramids. As evident from Figure 1(f), the spikes can completely be removed by annealing the film at 850 K, a temperature where the pyramidal structures are well preserved.

To explain the pyramidal surface structure, we assume that the nucleation of CeO_2 is templated by the substrate in triangles as it has been observed for the nucleation of Pr_2O_3 on Si(111)[26] and that the growth of the pyramidal structures is a kinetically limited process, similar to the one proposed for the growth of platinum on Pt(111).[27] Such structures, commonly referred to as "wedding cakes" develop during multilayer growth in the presence of a significant step edge barrier.[28,29] Atoms adsorbing on a terrace during MBE diffuse on this terrace but, in most cases, can not overcome the step edges due to the Ehrlich Schwoebel barrier.[30] Thereby the probability for adatoms to diffuse to a lower terrace is very small. This leads to a higher intra-layer diffusion than inter-layer diffusion and the synchronous growth of structures on all terrace levels. For the (111) surface of a fluorite type crystal, it is well known that two different kinds of

steps, namely, type I (A) and type II (B)[12,13] exist. For equal probability of particle attachment for type I and type II steps, we would expect a hexagonal shape for islands like in Figure 3(e). However, the probability of attachment at type I steps is higher, and, therefore, type II steps grow faster,[31] resulting in triangular rather than hexagonally shaped islands, as we observe them on the film. The change of the slope between the bottom and the top layers is attributed to a change in the Ehrlich Schwoebel barrier during the growth process. This growing mechanism results in the metastable surface morphology with the observed pyramidal structure that is stable for annealing temperatures up to 850 K. The low temperature morphology is also confirmed by spot profile analysis low energy electron diffraction (SPA-LEED) measurements revealing the threefold rotational symmetry corresponding to the tetrahedral pyramids.[32]

A significant change, namely, a transformation of the surface into the *high temperature morphology* occurs when annealing the film to a temperature of 930 K or higher. The onset of this transformation is shown in Figure 3(a). This image reveals terraces having a much larger contiguous area with (111) orientation than before. The width of the terraces is about 10 to 15 nm and thereby three times larger than the terraces on the pyramidal structures. The step height remains predominantly one triple layer while we also find some step edges with two and three triple layers height.

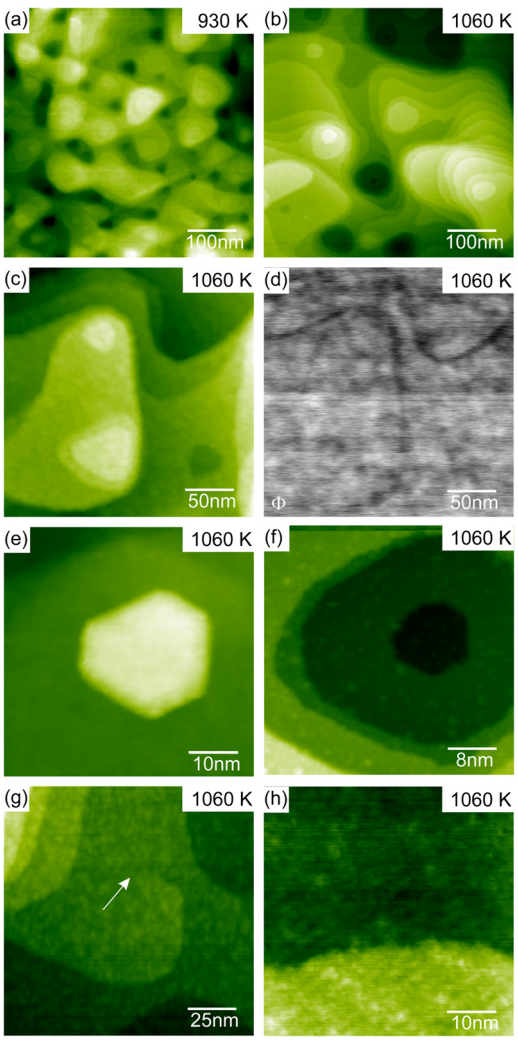

FIG. 3. Selected NC-AFM topography and KPFM (Φ) images taken after different post deposition annealing treatments representing the high temperature morphology. (a) Annealing at 930 K. (b)–(h) Annealing at 1060 K. The arrow in (g) marks a screw dislocation.

The transformation is completed after annealing the film at a temperature of 1060 K, where related images are shown in Figures 3(b)–3(h). In this state, the terraces on the surface have a width of 50 to 100 nm, and the average extension of the terraces on the film is, therefore, significantly larger than the extension of terraces on similarly prepared single crystal surfaces.[12,20,23] Compared to the situation for annealing at 930 K, we find more straight step edges, step edges with two, three, or four triple layer height, hexagonal protrusions, hexagonal pits, and screw dislocations (Figures 3(e)–3(g)), features that are well known from the bulk crystal surface.[12,20,23] Hence, at the nanoscale, the high temperature prepared surfaces of bulk and thin film ceria can hardly be discriminated from each other with the latter having larger terraces. The surface phase transition is confirmed by SPA-LEED.[32] However, high resolution NC-AFM imaging reveals many irregularities that appear on terraces and at step edges and can clearly be identified in Figures 3(g) and 3(h). Interestingly, they yield specifically strong local contrast features in Kelvin probe force microscopy (KPFM) images (see Figure 3(d)) indicating the presence of local charge or polarisation. Even when subjecting the sample to Ar^+ ion sputter cycles and annealing at a temperature of 1090 K (results not shown), the irregularities prevail. As surfaces of bulk ceria crystals can readily be prepared with much better atomic regularity using similar sputter/anneal cycles, we can exclude surface contaminants as the origin of the irregularities. We speculate that the irregularities are due to the reduction of the ceria film as X-ray photoelectron spectroscopy measurements[33] reveal that after annealing at 1060 K, near surface layers transform into Ce_7O_{12} and Ce_2O_3 is the phase finally stabilised at high temperatures.[33,34] Hence, the irregularities might result from oxygen vacancy clusters. The observation of a rapid increase of surface contamination upon exposure to the residual gas reported for the film system earlier[20] points to a certain reactivity and the attraction of contaminants by electrostatic interaction. Annealing temperatures over 1100 K yield a decomposition of the film related to Cer-silicide formation.[32]

In summary, we have shown that Cerium oxide films grown on hex-Pr_2O_3(0001)/Si(111) exhibit a metastable surface morphology consisting of terraced pyramids grown in [111] direction with the base oriented in the $[\bar{1}\,\bar{1}\,2]$ direction. When the film is subjected to post deposition annealing temperatures between 930 K and 1100 K, the pyramids undergo a phase transition into large terraces separated by steps with predominantly one O-Ce-O triple-layer height. The properties of the film surface then resemble those of well known ceria crystals, however, the film exhibit significantly larger terraces.

The authors are indebted to Philipp Maaß for a stimulating discussion on the ceria growth mechanism. Support by the Deutsche Forschungsgemeinschaft (DFG) via Grant Nos. WO 533/16-1, RE 1186/12-1, and SCHR 1123/4-1 and by the COST Action CM1104 is gratefully acknowledged.

[1]A. Trovarelli and P. Fornasiero, *Catalysis by Ceria and Related Materials*, 2nd ed., reprinted ed., Catalytic Science Series (Imperial College Press, 2013).
[2]H. S. Gandhi, G. W. Graham, and R. W. McCabe, J. Catal. **216**, 433 (2003).
[3]S. Torbrügge, M. Reichling, A. Ishiyama, S. Morita, and O. Custance, Phys. Rev. Lett. **99**, 056101 (2007).
[4]M. V. Ganduglia-Pirovano, J. L. F. Da Silva, and J. Sauer, Phys. Rev. Lett. **102**, 026101 (2009).
[5]C. J. Weststrate, R. Westerström, E. Lundgren, A. Mikkelsen, and J. N. Andersen, J. Phys. Chem. C **113**, 724 (2009).
[6]P. Luches, F. Pagliuca, and S. Valeri, J. Phys. Chem. C **115**, 10718 (2011).
[7]J. F. Jerratsch, X. Shao, N. Nilius, H. J. Freund, C. Popa, M. V. Ganduglia-Pirovano, A. M. Burow, and J. Sauer, Phys. Rev. Lett. **106**, 246801 (2011).
[8]F. Dvořák, O. Stetsovych, M. Steger, E. Cherradi, I. Matolínová, N. Tsud, M. Škoda, T. Skála, J. Mysliveček, and V. Matolín, J. Phys. Chem. C **115**, 7496 (2011).
[9]V. Stetsovych, F. Pagliuca, F. Dvořák, T. Duchoň, M. Vorokhta, M. Aulická, J. Lachnitt, S. Schernich, I. Matolínová, K. Veltruská, T. Skála, D. Mazur, J. Mysliveček, J. Libuda, and V. Matolín, J. Phys. Chem. Lett. **4**, 866 (2013).
[10]G. E. Murgida and M. V. Ganduglia-Pirovano, Phys. Rev. Lett. **110**, 246101 (2013).
[11]P. Luches, F. Pagliuca, S. Valeri, and F. Boscherini, J. Phys. Chem. C **117**, 1030 (2013).
[12]S. Torbrügge, M. Cranney, and M. Reichling, Appl. Phys. Lett. **93**, 073112 (2008).
[13]H. H. Pieper, C. Barth, and M. Reichling, Appl. Phys. Lett. **101**, 051601 (2012).
[14]N. Nilius, S. M. Kozlov, J. F. Jerratsch, M. Baron, X. Shao, F. Viñes, S. Shaikhutdinov, K. M. Neyman, and H. J. Freund, ACS Nano **6**, 1126 (2012).
[15]S. M. Kozlov, F. Viñes, N. Nilius, S. Shaikhutdinov, and K. M. Neyman, J. Phys. Chem. Lett. **3**, 1956 (2012).
[16]I. G. Danilova, E. M. Slavinskaya, V. I. Zaikovskii, A. S. Ivanova, A. I. Boronin, R. V. Gulyaev, and Y. I. Amosov, Kinet. Catal. **51**, 143 (2010).
[17]J. L. Lu, H. J. Gao, S. Shaikhutdinov, and H. J. Freund, Surf. Sci. **600**, 5004 (2006).
[18]A. Saywell, J. Schwarz, S. Hecht, and L. Grill, Angew. Chem., Int. Ed. **51**, 5096 (2012).
[19]M. H. Zoellner, J. Dabrowski, P. Zaumseil, A. Giussani, M. A. Schubert, G. Lupina, H. Wilkens, J. Wollschläger, M. Reichling, M. Bäumer, and T. Schroeder, Phys. Rev. B **85**, 035302 (2012).
[20]H. H. Pieper, C. Derks, M. H. Zoellner, R. Olbrich, L. Tröger, T. Schroeder, M. Neumann, and M. Reichling, Phys. Chem. Chem. Phys. **14**, 15361 (2012).
[21]J. V. Lauritsen and M. Reichling, J. Phys.: Condens. Matter **22**, 263001 (2010).
[22]S. Torbrügge, J. Lübbe, L. Tröger, M. Cranney, T. Eguchi, Y. Hasegawa, and M. Reichling, Rev. Sci. Instrum. **79**, 083701 (2008).
[23]S. Gritschneder and M. Reichling, Nanotechnology **18**, 044024 (2007).
[24]S. Gritschneder, Y. Namai, Y. Iwasawa, and M. Reichling, Nanotechnology **16**, S41 (2005).
[25]H. H. Pieper, C. Lammers, L. Tröger, S. Bahr, and M. Reichling, Rev. Sci. Instrum. **83**, 055110 (2012).
[26]L. Libralesso, T. Schroeder, T. L. Lee, and J. Zegenhagen, Surf. Sci. **598**, L347 (2005).
[27]M. Kalff, P. Šmilauer, G. Comsa, and T. Michely, Surf. Sci. **426**, L447 (1999).
[28]J. Krug, Physica A **313**, 47 (2002).
[29]I. V. Markov, *Crystal Growth for Beginners: Fundamentals of Nucleation, Crystal Growth and Epitaxy* (World Scientific, 2008).
[30]G. Ehrlich and F. Hudda, J. Chem. Phys. **44**, 1036 (1966).
[31]M. Einax, W. Dieterich, and P. Maass, Rev. Mod. Phys. **85**, 921 (2013).
[32]See supplementary material at http://dx.doi.org/10.1063/1.4866667 for details about the SPA-LEED measurements and the decomposition of the ceria film at high temperatures.
[33]H. Wilkens, O. Schuckmann, R. Oelke, S. Gevers, M. Reichling, A. Schaefer, M. Bäumer, M. H. Zoellner, G. Niu, T. Schroeder, and J. Wollschläger, Phys. Chem. Chem. Phys. **15**, 18589 (2013).
[34]H. Wilkens, O. Schuckmann, R. Oelke, S. Gevers, A. Schaefer, M. Bäumer, M. H. Zoellner, T. Schroeder, and J. Wollschläger, Appl. Phys. Lett. **102**, 111602 (2013).

APL Supplemental Material
A well-structured metastable ceria surface

R. Olbrich,[1] H. H. Pieper,[1] R. Oelke,[1] H. Wilkens,[1] J. Wollschläger,[1] M. H. Zoellner,[2] T. Schroeder,[2] and M. Reichling[1, a)]

[1)] *Fachbereich Physik, Universität Osnabrück, Barbarastr. 7, 49076 Osnabrück, Germany*

[2)] *IHP, Im Technologiepark 25, 15236 Frankfurt (Oder), Germany*

(Dated: 24 January 2014)

I. PHASE TRANSITION OF THE CERIA FILM OBSERVED BY SPA-LEED

The transformation of the surface from the low temperature morphology to the high temperature morphology is confirmed by spot profile analysis low energy electron diffraction (SPA-LEED) measurements. Figures 1(a) to (d) show representative SPA-LEED images after annealing the ceria film at low temperature (figure S1 (a) and (b)) and high temperature (figure S1 (c) and (d)). For the low temperature preparation, satellites can be observed close to the fundamental diffraction spots of zero and first order if the diffraction condition is appropriate.

The intensity distribution and shape of the diffraction spots as well as the satellites close to the fundamental diffraction spots exhibits the behaviour typical for a facet structure with threefold symmetry. While satellites appear for out-of-phase diffraction conditions, they disappear in crystallographic directions for in-phase diffraction conditions. At an electron energy of 95.3 eV, (close to the in-phase-condition for the (00) spot being equivalent to a 3D Bragg condition), the satellites close to the (00) diffraction spot almost vanish while the first order diffraction spots exhibit satellites since here the diffraction spots are not at in-phase diffraction condition (see figure S1 (a)). On the other hand, for 115.3 eV (close to the out-of-phase condition for the (00) spot), the (00) spot is clearly accompanied by satellites resulting from the facet structure while they are almost vanished for the first order diffraction spots. This is schematically illustrated in figure S2 showing the crystal truncation rods (CTR) from (111) plane diffraction and additionally the inclined Bragg rods corresponding to the facets. Satellites appear as streaks pointing away from the CTR in $\langle 1\ 1\ \overline{2}\ \rangle$ directions. The threefold rotational symmetry of the streaks corresponds to the tetrahedral shape of the pyramids as observed by NC-AFM for low temperature preparations. The streaky behaviour of the satellites is attributed to the large terrace extension of the (111) terraces on the facets in $\langle\ \overline{1}\ 1\ 0\ \rangle$ directions as well as to the short extension in $\langle 1\ 1\ \overline{2}\ \rangle$ directions. The uneven intensity distribution of the higher order diffraction spots resulting in the apparent threefold symmetry of the 2D diffraction intensity distribution are a result of the ABC stacking in the fcc based fluorite structure of ceria[1]. The diffraction patterns close to the in-phase and out-of-phase conditions of the (00) spot after annealing to high temperatures are shown in figure S1 (c) and (d). The satellites are absent for both diffraction conditions while the fundamental diffraction spot is sharp. This agrees well with the NC-AFM observation of large terraces. The size of these terraces is beyond the instrumental resolution

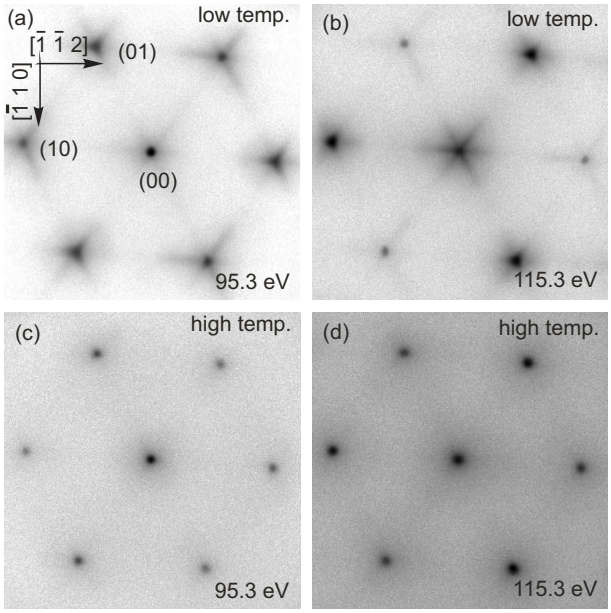

FIG. S1. Typical SPA-LEED diffraction patterns representing the low temperature morphology (a, b) and the high temperature morphology (c, d). The diffraction patterns are scaled to yield an equal size for the surface Brillouin zone of CeO_2(111). (a) represents the diffraction pattern close to the in-phase condition of the (00) spot while (b) represents the diffraction pattern close to the out-of-phase condition of the (00) spot. The shape of the streaks close to the fundamental diffraction spots show the behaviour typical for facets and is related to the tetrahedral structure of the pyramids observed by NC-AFM. The rounded spots in the diffraction pattern for annealing to higher temperatures shown in (c) and (d) are related to the dissolution of the pyramidal structure and the emerging wide terraces with (111) orientation since streaks appear neither for the (00) in-phase condition (c) nor the (00) out-of phase condition.

[a)] reichling@uos.de

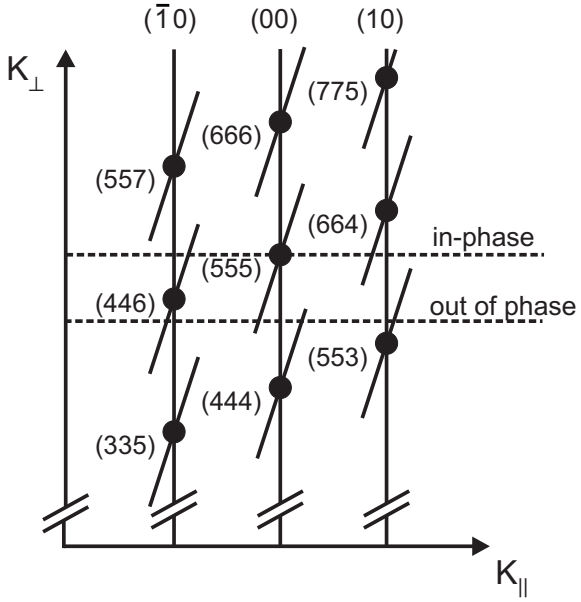

FIG. S2. Schematic drawing of the reciprocal space explaining the SPA-LEED results. The perpendicular component $K_\perp$ of the scattering vector is perpendicular to the (111) ceria surface. Thus the crystal truncation rods pointing in [111] direction are due to the (111) terraces. The facets yield additional tilted Bragg rods perpendicular to the surface of the facets. At 3D Bragg conditions (in-phase) the Bragg rods of the facets merge with the Bragg rods of the (111) terraces so that no satellites appear in the diffraction pattern close to the (00) rod. However, satellites are visible for first order diffraction rods. For out-of-phase condition the situation is vice versa: The satellites are pronounced for the (00) rod while they are almost vanished for the first order Bragg rods

of the SPA-LEED instrument so that the surface of the ceria film appears flat. The 3-fold symmetry of the intensity of the first order diffraction spots, however, is still visible indicating that the cubic symmetry of the ceria film and its ABC stacking is preserved.

II. DECOMPOSITION OF THE CERIA FILM

When the ceria film is annealed at temperatures higher than 1100 K, a dramatic change in the surface morphology appears as shown in the NC-AFM image of figure S3 (a). We observe hexagonally shaped hillocks with a lateral extension of several hundred nanometres separated by trenches. The height difference between the apparent bottom of the trenches and the highest points of the hillocks is of the order of 100 nm what is ten times more than the maximum height difference determined on the surface of films annealed at 1060 K. It is not possible to resolve any nanoscale or atomic scale details on the surface of the hillocks pointing to an amorphous structure or a contamination layer on the surface. We interpret the transformation from the terrace structure to the hillock structure as a decomposition of the ceria film accompanied by the formation of silicate and silicide. This interpretation is supported by measurements of the film bulk structure with X-ray diffraction, its near surface structure by low energy electron diffraction and its surface chemical composition by X ray photoelectron spectroscopy as reported elsewhere[2]. These studies also reveal a progressing reduction of the ceria film during extended heat treatment accompanying the morphological transformation. Transmission Electron Microscopy with Energy Dispersive X-Ray Analysis measurements taken after annealing the ceria film to 1270 K (data not shown) reveal the formation of large Cer-silicide islands completely depleted from oxygen. The optical properties of the film also reflect the different temperature regimes as shown in the photographic images of figure S3 (b) taken after annealing at 300 K, 1060 K and 1150 K.

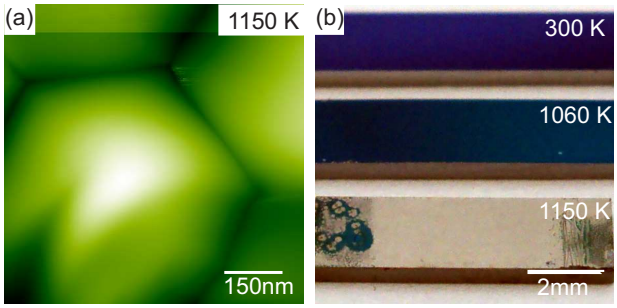

FIG. S3. NC-AFM topography image (a) revealing the decomposition of the ceria film after annealing to 1150 K and visual impression (b) of the film after heat treatment at different temperatures visualising significant changes in the optical properties of the film when passing critical temperatures.

[1] M. H. Zoellner, J. Dabrowski, P. Zaumseil, A. Giussani, M. A. Schubert, G. Lupina, H. Wilkens, J. Wollschläger, M. Reichling, M. Bäumer, and T. Schroeder, Phys. Rev. B **85**, 035302 (2012).
[2] H. Wilkens, O. Schuckmann, R. Oelke, S. Gevers, M. Reichling, A. Schaefer, M. Bäumer, M. H. Zoellner, G. Niu, T. Schroeder, and J. Wollschläger, Phys. Chem. Chem. Phys. **15**, 18589 (2013).